ELSEVIER

Earth and Planetary Science Letters 171 (1999) 351–365

EPSL

www.elsevier.com/locate/epsl

# Thermal constraints on the survival of primitive blobs in the lower mantle

Thorsten W. Becker *, James B. Kellogg, Richard J. O'Connell

*Harvard University, Department of Earth and Planetary Sciences, 20 Oxford Street, Cambridge, MA 02138, USA*

Received 16 November 1998; revised version received 7 May 1999; accepted 7 June 1999

**Abstract**

Geochemical models have frequently divided the mantle into depleted upper and undepleted lower mantle reservoirs, usually taken as indication for a layered style of convection. This is difficult to reconcile with seismological and geodynamical evidence for substantial mass flux between lower and upper mantle. Various models have been proposed to jointly interpret the evidence, including that of G.F. Davies [J. Geophys. Res. 89 (1984) 6017–6040] in which the author suggested that lumps of primitive material may exist in the lower mantle, representing reservoirs for undepleted basalts. Mixing calculations have suggested, however, that such blobs could not survive 4 Ga of convection. Calculations by M. Manga [Geophys. Res. Lett. 23 (1996) 403–406] on the other hand showed that high-viscosity blobs could persist in convective cells for geologically long times without being substantially deformed and mixed with the surrounding flow. We investigate a blob model of convection based on these ideas and consider dynamical, thermal, geochemical and rheological consequences. The radiogenic heat production in the primitive blobs would lead to higher temperatures. However, these would be modest ($\Delta T < 300$ K) for sufficiently small blobs (radius <800 km). The resulting thermal buoyancy can be offset by a small intrinsic density excess (<1%) so that blob material is hidden from the ridges but sampled by rising plumes. To satisfy geochemical constraints, blobs would have to fill 30% to 65% of the mantle (less if they are taken to be enriched rather than primitive). Thermal considerations require that they be surrounded by depleted material of lower viscosity that would convectively transport heat to the surface. The thermal decrease in blob viscosity would be about one order of magnitude but constrained to the interior; the stiffer 'shell' can then be expected to control the dynamical mixing behavior. On average, the viscosity of the lower mantle would be increased by the presence of the blobs; if they were 100 times more viscous than the surrounding mantle the net effect would be to increase the effective viscosity approximately 5-fold. The origin of the proposed blobs is an unresolved problem. We suggest that perovskite/magnesiowüstite ratio variations could be the reason, which would yield an intrinsic density contrast as well. Blob geometries are at the current resolution limit of global tomographic models, and the trade-off between temperature and compositional effect on seismic wave speeds tends to blur the signal. However, joint P- and S-wave inversions and scattering studies may ultimately approach the necessary precision to detect blobs. Under the simplifying assumptions employed in this paper, we find that the viscous blob model is internally self-consistent and feasible. The model may explain the outstanding problem of incongruous geochemical and geophysical data. 

*Keywords:* convection; models; isotopes; mantle; noble gases; convection

* Corresponding author. Tel.: +1-617-495-8986; Fax: +1-617-495-8839; E-mail: becker@eps.harvard.edu

0012-821X/99/$ – see front matter 
PII: S0012-821X(99)00160-0

## 1. Introduction

Geochemical studies imply that the Earth's mantle is heterogeneous on all length scales [1–3], although the isotopic variability may be accounted for by a small number of end-member reservoirs [4]. Evidence for the existence of these reservoirs is strong, but constraints on the geometry are very weak. The presence of generally high $^3He/^4He$ ratios in Ocean Island Basalts (OIBs) associated with mantle plumes [5,6] is commonly interpreted as evidence for the existence of a primitive mantle. Scatter of $^3He/^4He$ ratios for different OIBs [7] is an indicator that the source region of these samples is much more heterogeneous than that of the mid-oceanic ridge basalts. The spatial stability of mantle plumes hint at a deep source, possibly the lowermost mantle. Box models of the formation of continental crust [8] suggest that the volume of the depleted mantle is comparable to the upper mantle. Furthermore, the global $^{40}Ar/^{40}K$ budget of the Earth can be used to argue for layered mantle convection. If the upper mantle is identified with the depleted mantle, the lower mantle then serves as the primitive reservoir of Ar/K, and there is low mass flux across the 670-km-discontinuity [9]. This is probably the strongest, although not undebated [10], argument of geochemistry for layered convection.

These geochemical observations are at odds with growing evidence from seismology and geodynamics. Studies [11,12] show a high mass flux across the transition zone and opt for a whole mantle style of convection. This is in accord with recent seismic tomography [13,14] which detects linear high-velocity anomalies continuing into the lower mantle, strongly suggesting slab penetration. Thus, with exceptions [15], geochemists have argued for a layered mantle throughout most of Earth's history, whereas geophysicists, working from different sets of data, have supported a whole-mantle picture.

In light of these two lines of evidence, it is apparent that neither end-member scenario is tenable and one must appeal to more exotic models. One such model is the penetrative convection picture of Silver [16], in which upper mantle material is intrinsically less dense than lower mantle material, but not enough so to overcome the negative buoyancy associated with cold slabs. Downgoing material, then, penetrates the lower mantle, equilibrates thermally, and returns preferentially to the upper mantle. Unfortunately, this model contains many of the weaknesses of the two-layer mantle, including the necessary presence of a thermal boundary layer at or near the 670-km-discontinuity, which is not likely to be present [17].

Davies [18] proposed instead a model in which there is no fundamental bias between the upper and lower mantle except an increase in viscosity, as suggested independently on the basis of geoid modeling [19]. Enriched or undegassed blobs of material are then dispersed throughout the mantle and sampled periodically by upwelling plumes. This model questions not the picture of a multi-reservoir Earth drawn by geochemistry but the standard geometry. Numerical studies of mixing, however, indicate that these blobs of material are unlikely to remain coherent over sufficiently long time scales. The high viscosity and low strain rates of the lower mantle appear to be an attractive way out of this problem [20]. Yet, in the absence of an intrinsic density contrast, any material in the lower mantle must ultimately be cycled through the upper mantle. There blobs will be subjected not only to the effects of lower viscosity [21], but also of toroidal motion [22,23].

On the other hand, using two-dimensional Stokes flow calculations with kinematic boundary conditions, Manga [24] showed that high-viscosity blobs can sustain multiple convective overturns virtually unstrained. This means that the time scales for blob erosion and mixing of blob material can be comparable to the geochemical age; stiffer regions could resist mixing with the surrounding mantle material over geologically long times when they had a viscosity higher by a factor of about 75. Furthermore, these blobs tend to aggregate in the low strain rate cores of convection cells and resist sampling at spreading centers [25]. If an intrinsic viscosity contrast were to remain sufficiently high over geological times, then these blobs could represent the dispersed reservoir envisioned by Davies and required by geochemistry (cf. Fig. 1).

Our goal here is to examine the dynamical and thermal persistence of these blobs, and give reasonable numbers for their size by order of magnitude

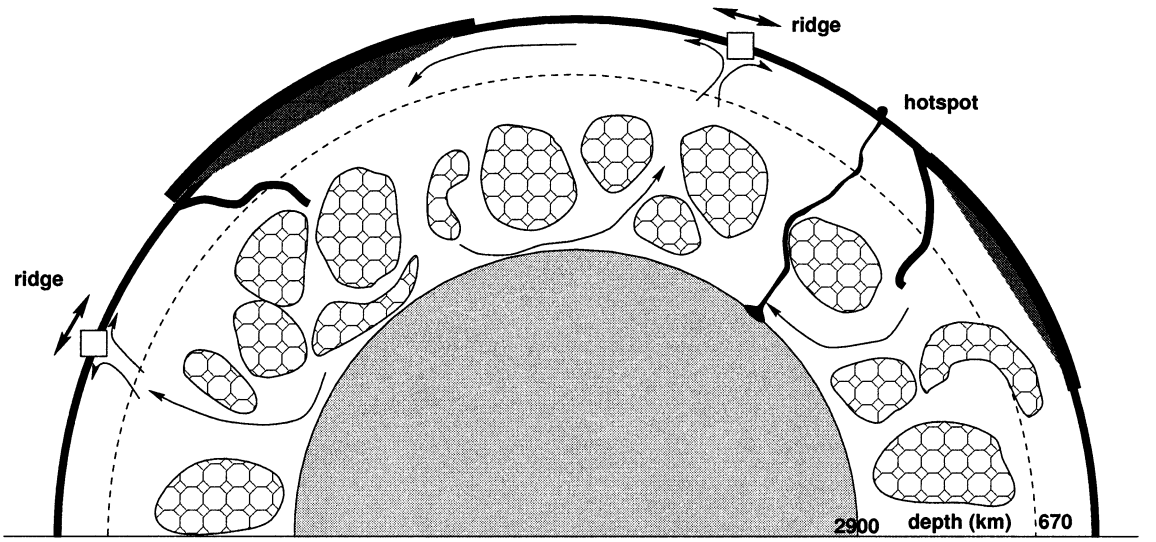


Fig. 1. The blob model of convection (cartoon). Note the following features: Convection is in the whole mantle mode with varying morphology of slab penetration through the 670-km-transition zone. The blobs reside mainly in the cores of the convective cells and represent the primitive reservoir. Surrounding material and especially the upper mantle region are depleted and degassed by melting at the ridges and earlier continent-formation. Blobs are sampled by rising plumes that entrain material and lead to a heterogeneous OIB isotope source.

calculations. The constraints we consider are shown not to violate the model.

## 2. Thermal constraints on blob dynamics

Radiogenic heating within the primitive blobs and the resulting viscosity reduction could overcome the hypothetic intrinsic viscosity contrast central to our argument. We present constraints on the following questions in an attempt to resolve some of the related issues. What might be the dominant mode of heat transport in a blob-filled mantle? How does the necessity to remove heat constrain the maximum fraction of blobs to depleted mantle volume? How high does the intrinsic negative buoyancy need to be to keep blobs from rising? What internal radiogenic temperature increase can be expected in the blobs and what follows for the viscosity reduction? Finally, what is the overall viscosity increase in a blob-filled mantle?

### *2.1. Conductive versus convective cooling*

For simplicity, we consider heat transport around a fixed, rigid and internally heated sphere of radius $a$ within an open streamline flow of background convective velocity $u_\infty$. Any time-dependent reconfiguration of the convective pattern that might be due to moving ridges or unsteady plumes is not included in such an analysis.

We assume that the temperature at the surface of the sphere is kept at constant ambient temperature, $T_a$, and investigate the validity of this assumption in the following. For this to work, the temperature of the material passing over the surface of the sphere must not increase significantly, but rather the material has to be advected away before heating up. In other words, the convective time scale must be shorter than the conductive. The Peclet number, Pe, is the ratio between these two numbers and defined by:

$$\mathrm{Pe} = \frac{u_\infty a}{\kappa} \tag{1}$$

where $\kappa$ is the thermal diffusivity. If we take characteristic values for the lower mantle (cf. Table 1), and a blob radius of $a = 50$ km — later shown to be reasonable — we get $\mathrm{Pe} = \mathcal{O}(200)$ for most estimates of $u_\infty$. Thus we expect the time scales of conduction to be significantly shorter than those of convection

Table 1
Summary of the parameters used and derived in this study

| Parameter | Value | Reference |
|---|---|---|
| Thermal conductivity | $k = 8.5$ W m$^{-1}$ K$^{-1}$ | [26, p. 459] |
| Thermal expansivity | $\alpha = 1.4 \times 10^{-5}$ K$^{-1}$ | [26, p. 459] |
| Heat capacity | $C_p = 1270$ J kg$^{-1}$ K$^{-1}$ | [26, p. 459] |
| Mean density | $\rho_0 = 4903$ kg m$^{-3}$ | [27] |
| Characteristic velocity of convection | $u_\infty = 1.5$ cm yr$^{-1}$ | [17] |
| Activation energy | $H = 600$ kJ mol$^{-1}$ | [28, p. 333] |
| Ambient temperature | 2000 K $\leq T_a \leq$ 4000 K | [26, p. 459] |
| Characteristic blob radius | 550 km $\leq a_c \leq$ 780 km | Eq. 10 |
| **Derived quantities** | | |
| Thermal diffusivity | $\kappa = 1.4 \times 10^{-6}$ m$^2$ s$^{-1}$ | $k/(C_p\rho)$ |
| Peclet number | 191 $\leq$ Pe $\leq$ 271 | Eq. 1 |
| Heat production rate | $A_0 = 2.5 \times 10^{-8}$ W m$^{-3}$ | Table 2 |
| Characteristic half-distance between the blobs | 96 km $\leq b \leq$ 121 km | Eq. 3 |
| Maximum surplus temperature | 150 K $\leq \Delta T_{max} \leq$ 300 K | Eq. 8 |
| Maximum viscosity reduction | $0.5 \leq \eta_{min} \leq 0.009$ | Eq. 14 |

The values are thought to be representative of lower mantle conditions at present time in Earth's history. When we used a range of values this is indicated.

around the blobs. In addition, the material flowing around the blobs will be removed more easily due to its thermally reduced viscosity and increased buoyancy. These effects support our assumption of an isothermal boundary condition in all that follows.

The extension of the diffusive boundary layer $l_d$ from the sphere into the convective system scales as $l_d \propto \sqrt{\kappa t_c}$, where $t_c$ is the characteristic contact time for material flowing by. For a bubble with a stress-free boundary condition, we would just use $t_c \propto a/u_\infty$. However, since we are considering the end-member case of a rigid sphere, the appropriate characteristic velocity is $u_\infty l_d/a$ and we get:

$$t_c \propto \frac{a^2}{u_\infty l_d} \tag{2}$$

instead. If the blobs get too close together, our assumption of convection as an effective method of heat transport breaks down. Therefore, we take as the minimum half-distance between blobs the characteristic diffusion length $b$ (cf. Fig. 2):

$$b \geq a\,\mathrm{Pe}^{-1/3} \tag{3}$$

Obviously, there is no force preventing the blobs from moving closer than $b$. However, if they do so, it is more appropriate from a thermal standpoint to consider them as a single, larger blob.

### 2.2. Geometrical constraints

With the constraints on $b$ from above we can now estimate the maximum volumetric ratio $f_b$ of blob material to ambient mantle when a fraction $C$ of the total mantle volume can be filled with blobs. Note that $b$ is not meant to represent a mean distance between the blobs, but rather a minimum distance indicating the conditions under which our assumptions about heat flow hold. One way to approximate the blob geometry (case A) is by calculating the volume of spheres separated by a distance $2b$ in cubes. This should be appropriate when we think of small and isolated blobs. Then the volume fraction as a function of blob radius $a$ is given by:

$$f_b^A = C\frac{\pi}{6}\frac{a^3}{(a+b)^3} \tag{4}$$

where $b$ is given by Eq. 3. We do not take the annulus-shaped mantle geometry or a blob size distribution into account. A more extreme set-up (case B), which is more appropriate if the blobs are imagined to fill the whole interior of a convective cell, is realized by cubes with half side length $a$ (Fig. 2, B), so that:

$$f_b^B = C\frac{a^3}{(a+b)^3} \tag{5}$$

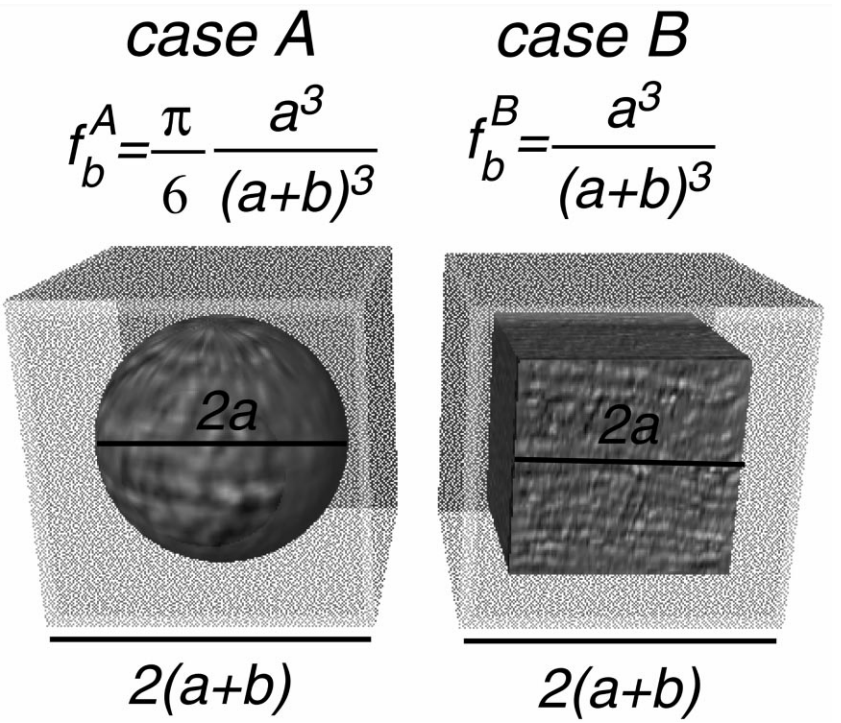


Fig. 2. Simplified blob geometry for volume filling considerations. $f_b^{A,B}$ indicates the volume fraction of $V_b/V_m$ for end-members A and B.

Obviously, the large-scale blobs are more efficient in terms of volume filling. Case B can be viewed as an equivalent of case A when the missing 'corners' of the $8(a+b)^3$ cube are allowed to be filled by a size-distribution of smaller, spherical blobs. We note that Manga's calculations [24] indicate that blobs will not stay perfectly separated for all times but coalesce and separate again. In this respect, we are considering an average blob size. The considerations on blob geometry further remind us that our blob model lies on a continuum between isolated, small lumps and large-scale rheological stratification depending on the volume fraction $f_b$.

Fig. 3 shows the volume fractions predicted by Eqs. 4 and 5. They are calculated by taking the equality in Eq. 3 and substituting the numbers of Table 1. The plot demonstrates that the dependence on $a$ is not very pronounced and a significant fraction of the mantle volume can be occupied by primitive material in our model. We will choose characteristic radii and discuss the implications of the estimates shown in Fig. 3 in terms of geochemical mass balances below.

### 2.3. Internal temperature in the primitive blobs

We now examine further thermal constraints on the blob size. A consequence of the more primitive composition of the blobs is a higher rate of internal heat production than in the surrounding matrix. Thus, the blobs can be expected to heat up, possibly increasing their buoyancy to a point at which they congregate not at the cores of convection cells but rather at the shallowest levels of the mantle. To evaluate this possibility, we begin by calculating a reasonable value for the volumetric heat production rate, $A_0$, in the undepleted blob material.

### 2.4. Assessing the heat production

To calculate the rate of internal heating, we assume relative and absolute abundances of radiogenic elements for the bulk silicate Earth that are based on [29] (cf. Table 2). Combining these with heat generation values given in [26] we find that the resulting heat generation of the bulk silicate Earth is

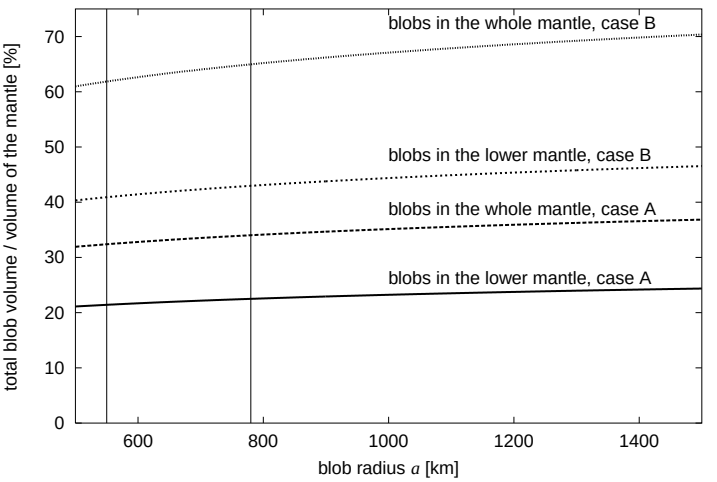


Fig. 3. Fraction of the mantle volume that is occupied by blobs vs. blob radius $a$ for cases A and B. The average distance between blobs, $2b$, was calculated from the thermal constraint of Eq. 3. The two vertical lines correspond to characteristic blob radii of 550 km and 780 km. Labels 'lower' and 'whole' mantle correspond to $C$ values of 0.66 and 1, respectively.

$5.1 \times 10^{-12}$ W/kg, about the same as for carbonaceous chondrites. In the depleted mantle, the majority of the heat-producing elements have been lost by fractionation to the continental crust. Yet, the blobs hold their original composition to first order, with possible depletion or enrichment due to entrainment of ambient mantle or delaminated crustal material, respectively. We assume for our model, therefore, that the blobs produce heat at the rate cited above. Taking the average density for the lower mantle $\rho_0 = 4903$ kg/m$^3$ [27], we arrive at the volumetric rate of heat production in the blobs:

$$A_0 = 2.5 \times 10^{-8} \ \text{W/m}^3 \tag{6}$$

We take this value as a reference and show how our results depend on variations in $A_0$.

Table 2
Abundances of radiogenic elements in the bulk silicate Earth from [29]

| | | |
|---|---|---|
| Uranium abundance | U | 20.3 ppb |
| Uranium isotope ratio | $^{238}$U/$^{235}$U | 137.88 |
| Thorium abundance | Th | 79.5 ppb |
| Potassium abundance | K | 240 ppm |
| Potassium isotope ratio | $^{40}$K/K | $1.17 \times 10^{-4}$ |

### 2.5. Conductive solution for an internally heated sphere

We proceed to estimate the excess temperature $\Delta T$ within the blobs due to the heat production rate $A_0$. Our approach is based on the argument outlined above that convective cooling is an effective mechanism outside the blobs and the temperature is constant on the surface. Therefore, we solve the heat diffusion equation for a solid sphere in an infinite medium with the boundary condition $\Delta T(r = a) = 0$ for all times $t$. Choosing the initial condition $\Delta T(t = 0) = 0$ for all $r$, the full solution is [30]:

$$\frac{\Delta T(\overline{r}, \overline{t})}{\Delta T_{\max}} = (1 - \overline{r}^2) + \frac{12}{\pi^3 \overline{r}} \times \sum_{n=1}^{\infty} \frac{(-1)^n}{n^3} \sin(\pi n \overline{r}) \exp(-\pi^2 n^2 \overline{t}) \tag{7}$$

with

$$\Delta T_{\max} = \frac{A_0 a^2}{6k} \tag{8}$$

and $\overline{r} = r/a$, $\overline{t} = t/t_{\mathrm{d}}$ and $t_{\mathrm{d}} = a^2/k$. Here, $k$ is the thermal conductivity of the blob material, $r$ the distance from the center of the blob and $t_{\mathrm{d}}$ the diffusion time which is around 6.9 Ga for the numbers of Table 1 and a characteristic value for the radius parame-

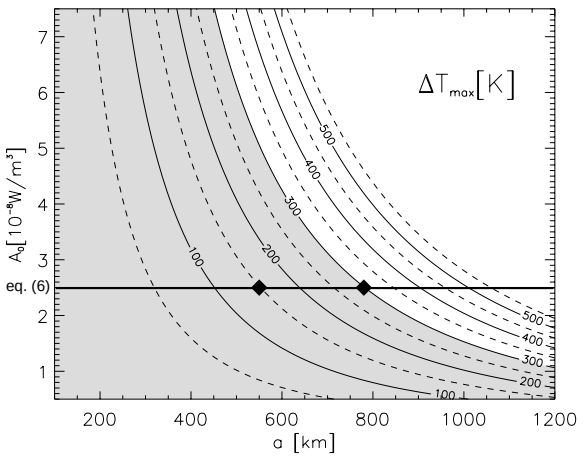


Fig. 4. Maximum temperature in the center of a blob ($\overline{r} = 0$) in degrees K as predicted by Eq. 8. Isotherms are shown from 50 K $\leq \Delta T_{\max} \leq$ 550 K in 50 K-intervals in a volumetric heat production rate vs. blob radius plot for $k = 8.5$ W m$^{-1}$ K$^{-1}$. We have indicated the parameter range for which $T_{\max} \lesssim 300$ K by shading. The two diamond-shaped symbols belong to the radii of $a = 550$ km and $a = 780$ km which for $A_0 = 2.5 \times 10^{-8}$ W/m$^3$ (Eq. 6) correspond to $T_{\max} \approx 150$ K and $T_{\max} \approx 300$ K, respectively.

ter $a$ of 550 km. It is not clear which initial condition is the appropriate one for the formation of primitive blobs. However, a closer inspection of Eq. 7 shows that the full solution approaches the parabolic shape of the steady-state temperature distribution for times $t \gtrsim 0.1$, albeit with a smaller maximum temperature increase. $\Delta T_{\max}(\overline{t}) = \Delta T(\overline{r} = 0, \overline{t})$ is around 70% and 93% that of the steady-state solution ($t \to \infty$) for $\overline{t} = 0.14$ (corresponding to 1 Ga) and $\overline{t} = 0.29$ (equivalent to 2 Ga), respectively. We hence neglect any transient effects and use the steady-state solution, noting that the resulting numbers for $\Delta T$ are upper bounds for the actual temperature increase one would expect.

The raised temperature within the blobs produces two effects: increased buoyancy due to thermal expansion and decreased viscosity within the blob. Fig. 4 shows the maximum temperature increase in the center of the blob as a function of $A_0$ and $a$. The temperature increase within the blobs will be moderate for a wide range of parameters. Choosing 300 K arbitrarily as a limit based on viscosity considerations which follow below, we get a corresponding blob radius of $a \approx 780$ km for our reference $A_0$.

We note that we have taken a rather conservative approach in estimating the temperature increase. For one thing, deviations from spherical shape would lead to more efficient heat transport. Furthermore, internal convection velocities for a non-rigid blob can be expected to be lower than $u_\infty$ by a factor corresponding to the inverse of the viscosity increase. Internal flow will hence be a secondary mechanism for high-viscosity blobs but might nevertheless lead to a flatter temperature profile than indicated by Eq. 7.

### 2.6. Buoyancy constraints

We can estimate the thermal buoyancy due to the excess heat inside a blob by integrating over the steady-state temperature profile Eq. 7:

$$\Delta\rho_{\mathrm{t}} = \frac{3\rho_0^{\mathrm{b}}\alpha}{a^3}\int_0^a \Delta T(r) r^2\,\mathrm{d}r \tag{9}$$

to obtain the condition for the dominance of intrinsic over thermal buoyancy:

$$\frac{\Delta\rho_{\mathrm{i}}}{\rho_0} > \frac{2}{5}\alpha\Delta T_{\max} \tag{10}$$

Here, $\alpha$ denotes the thermal expansivity, $\Delta\rho_{\mathrm{t}}$ and $\Delta\rho_{\mathrm{i}}$ the thermal and intrinsic density differences, respectively; $\rho_0^{\mathrm{b}}$ and $\rho_0$ denote the blob density and ambient mantle density. We used $\rho_0^{\mathrm{b}} \approx \rho_0$.

Assuming that blobs tend to congregate in the low strain-rate centers of convective cells, Eq. 10 describes the conditions under which thermal buoyancy will not drive the blobs up and out of these stable regions. However, if we wish to estimate the conditions under which all blobs of significant size remain in the lower mantle, we need to take the viscous drag into account which would tend to carry blobs caught in upwellings into the upper mantle. Such a correction leading to a higher intrinsic density requirement will also be of importance when a time-dependent, more vigorous style of convection is considered. If we introduce a second effective density contrast, $\Delta\rho_{\mathrm{s}}$, by means of the Stokes velocity:

$$u_{\mathrm{s}} = \frac{2}{9}\frac{\Delta\rho_{\mathrm{s}} g a^2}{\mu_{\mathrm{m}}} \tag{11}$$

Eq. 10 can be extended with the new density con-

straint to arrive at:

$$\frac{\Delta\rho_i}{\rho_0} \gtrsim \frac{\Delta\rho_s + \Delta\rho_t}{\rho_0} = \frac{9}{2}\frac{\mu_m u_s}{\rho_0 g a^2} + \frac{A_0 \alpha a^2}{15k} \qquad (12)$$

Here, $g$ denotes gravitational acceleration and $\mu_m$ is the viscosity of the ambient mantle. If we assume a blob radius $a = 780$ km, a viscosity of $\mu = 5 \times 10^{22}$ Pa s, $u_s = u_\infty$ and the material parameters of Table 1, then the first term on the right of Eq. 12 is on the same order as the second (cf. Fig. 5). Thus, viscous drag could be an important consideration, depending on the constraints one imposes on the blobs. However, as shown by Fig. 5, when blobs get larger they are more strongly affected by the thermal effect since it gets increasingly difficult to move them by viscous drag. In any case, the two terms on the right side of Eq. 12 never add up to more than 1% for $a \gtrsim 490$ km for our steady-state convection picture. In the following, we do not require the blobs to remain in the lower mantle, but rather consider only the conditions under which they may stay neutrally (or negatively) buoyant within convective cores. Therefore the basic Eq. 10 will be utilized as a constraint for $a$.

Fig. 5 demonstrates that the thermal buoyancy is balanced by small intrinsic density contrasts of the order of one percent even for very large blobs of whole mantle size. This is due to the temperature distribution which gives the volumetric factor of 2/5 in Eq. 10. Hence, Eq. 10 imposes only weak constraints on our model if we can find a mineralogical composition that can account for a high viscosity and a slightly higher density of ~0.5%. The finding that a large temperature difference is needed to overcome intrinsic negative buoyancy is supported by mineralogical studies for a pyrolite lower mantle [31].

### 2.7. Thermal reduction in blob viscosity

There will be a range of parameters for which the intrinsically higher viscosity of the blobs will play an important role in controlling the mixing dynamics. A commonly used temperature and stress dependent creep law for rocks is:

$$\dot{\varepsilon} = E\tau^n \exp\left(-\frac{H}{RT}\right) \qquad (13)$$

Here, $\dot{\varepsilon}$ denotes the strain rate, $E$ a constant, $\tau$ the shear stress, $n$ the power-law exponent (around 3), $H$ a lumped thermal activation energy, and $R$ the gas constant. We have neglected grain size and pressure dependence (where $H$ is replaced by the enthalpy $H + pV_a$) since their importance in the

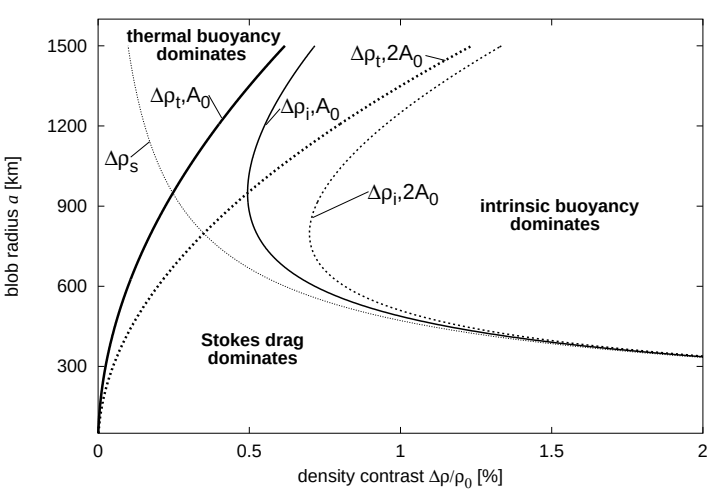


Fig. 5. Maximum blob size as of buoyancy conditions (Eqs. 10 and 12). Areas to the left of the lines denoted '$\Delta\rho_t$' mark the region in parameter space for domination of thermal over intrinsic buoyancy, Eq. 10, for $A_0$ and $2A_0$. Taking Stokes drag into account, Eq. 11, the line marked '$\Delta\rho_s$' forms the upper bound to systems where blobs are much influenced by the background flow for $u_s = u_\infty = 1.5$ cm/yr and $\mu_m = 5 \times 10^{22}$ Pa s. Finally, '$\Delta\rho_i$' lines confine the areas where the intrinsic buoyancy counterbalances both effects, Eq. 12. Note that thermally rising blobs of all sizes permitted by the Earth's mantle are rendered neutrally buoyancy by an intrinsic density contrast of $\mathcal{O}$(1%). The same holds true for the Stokes drag when considering blobs with $a > 490$ km.

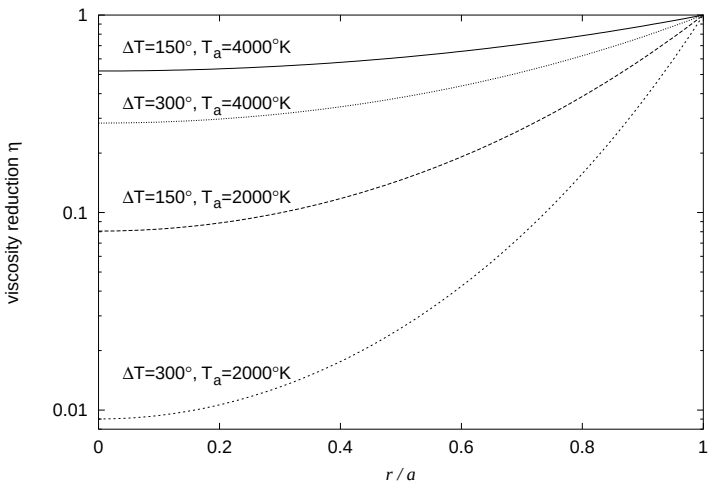


Fig. 6. Viscosity reduction $\eta$ inside the blobs for maximum blob temperature 150 K $\leq \Delta T_{\max} \leq$ 300 K (corresponding to 550 km $\leq a \leq$ 780 km) and background mantle temperature 2000 K $\leq T_a \leq$ 4000 K. We show reduction relative to a blob reference which is proposed to be itself higher than the ambient mantle.

deep mantle is still debated and might be small [28]. We furthermore take $H = 600$ kJ/mol as a characteristic value for perovskite-like minerals (cf. Table 1). Assuming constant stress, we can then write the reduction in blob viscosity, $\eta$, when the temperature is increased from $T_a$ to $T_a + \Delta T$ as:

$$\eta(\overline{r}) = \frac{\mu(T_a + \Delta T(\overline{r}))}{\mu(T_a)} = \exp\left(\frac{H}{R\,(T_a + \Delta T(\overline{r}))} - \frac{H}{RT_a}\right) \qquad (14)$$

where the dynamic viscosity is defined by $\mu = \tau/\dot{\varepsilon}$. As noted by Karato [32], this procedure gives maximal weight to the temperature dependence. If we would have chosen constant strain rate or constant viscous dissipation instead, $H$ — and thus the temperature dependence in Eq. 14 — would have been reduced by a factor of $1/n$ or $2/(n+1)$.

To arrive at a quantitative estimate, we show $\eta$ in Fig. 6 for different values for $\Delta T_{\max}$ and $T_a$. The maximum blob temperatures used, $\Delta T_{\max} = 150$ K and $\Delta T_{\max} = 300$ K, correspond to $a = 550$ km and $a = 780$ km, respectively (Eq. 8) while the background mantle temperature $T_a$ is varied from 2000 K to 4000 K. These numbers are characteristic values for the lower mantle. Fig. 6 indicates that the reduction in viscosity is less than or about one order of magnitude for most of the parameter values; only low $T_a$, high $\Delta T_{\max}$ end-members result in extreme reduction of $\eta_{\min} = \eta(\overline{r} = 0) = 0.009$.

Fig. 6 also illustrates the radial viscosity structure within the blobs. The regions most affected by internal heating and therefore least viscous are restricted to within about half the radius (~13% of the volume) of the blobs. The outer shell maintains a viscosity close to the maximum as established by the ambient mantle temperature and intrinsic viscosity increase. Preliminary numerical calculations for blobs with a hard outer shell and a weak interior lead us to conjecture that even if the viscosity is reduced substantially in the interior of the blobs (say, up to half the radius), mixing might still be significantly slowed down by the proposed intrinsic stiffness.

A related issue is viscous dissipation $\Phi$ during the motion of blobs. Dissipative heating will be pronounced at the interface between the hard blob shell and the surrounding weaker mantle material and might lead to thermal erosion from the outside. $\Phi$ scales as $\tau^2/\mu$ and will be only about 1% of $A_0$ when we take $\tau = 1$ MPa and $\mu = 5 \times 10^{22}$ Pa s as typical numbers for the mantle. However, numerical models have shown that viscous heating can become an important factor due to interaction with non-linear rheology [33]. While the significance of this effect for our model remains to be determined, we note that viscous heating might facilitate the entrainment of primitive blob material in rising plumes, especially

since we are considering highly viscous material with a probably higher melting temperature.

### 2.8. The effective viscosity of the mantle

We estimate how the average viscosity can be expected to change in the lower mantle when it is partially filled with high-viscosity blobs. To calculate average properties of a composite medium, we utilize the solution for an isotropic two-material dispersion of viscoelastic spheres of volume fraction $f$ in a viscoelastic matrix [34]. We find:

$$\mu_{\mathrm{eff}} = \frac{1}{6}\left\{(5f-2)\mu_{\mathrm{b}} + (3-5f)\mu_{\mathrm{m}} + \left[24\mu_{\mathrm{b}}\mu_{\mathrm{m}} + ((5f-3)\mu_{\mathrm{m}} + (2-5f)\mu_{\mathrm{b}})^2\right]^{1/2}\right\} \quad (15)$$

for the effective viscosity $\mu_{\mathrm{eff}}$. Here, $\mu_{\mathrm{b}}$ and $\mu_{\mathrm{m}}$ are the viscosity of the blobs and the surrounding mantle respectively. Fig. 7 shows $\mu_{\mathrm{eff}}$ for different average blob viscosities. We chose to focus on the lower mantle whereas Eq. 15 is, of course, a general approximation for an effective viscosity.

Taking the case A geometry, $a = 780$ km and restricting blobs to the lower mantle, Eq. 4 yields a (whole mantle) $f_{\mathrm{b}}^{\mathrm{A}}$ of 23%. This means that 34% of the lower mantle volume is filled with blobs. Eq. 15 then predicts an effective viscosity increase of around 5 when the average blob viscosity contrast can be maintained at $\mu_{\mathrm{b}}/\mu_{\mathrm{m}} = 100$. When we choose geometry B for higher ratios of primitive to depleted mantle instead, we arrive at an average viscosity increase on the order of 40. Models, e.g. [19], usually show a viscosity increase on the order of 50 in the lower mantle that could result jointly from the phase-transition of olivine and the inclusion of stiffer blobs.

## 3. Discussion

The calculation of the thermal buoyancy demonstrated that blobs with a modest intrinsic density contrast will not rise due to their thermal buoyancy. We can therefore consider the whole mantle for blob placement since they will not necessarily get sampled at the ridges. Since the most important thermal constraint on blob size is the internal viscosity decrease, Eq. 14, we have chosen $a = 550$ km and $a = 780$ km as representative values that yield $\Delta T_{\mathrm{max}} \approx 150$ K and $\Delta T_{\mathrm{max}} \approx 300$ K as upper bounds. For these values, the viscosity reduction $\eta$ will probably be small enough so that the envisioned primitive blob reservoirs stay relatively unmixed over geological time.

### 3.1. Geochemical and heat flow constraints

Fig. 3 shows that the blob volume for the characteristic radii sums to roughly one (two) third(s) of the total mantle volume for case A (case B) if we consider the whole mantle for the blobs and use the

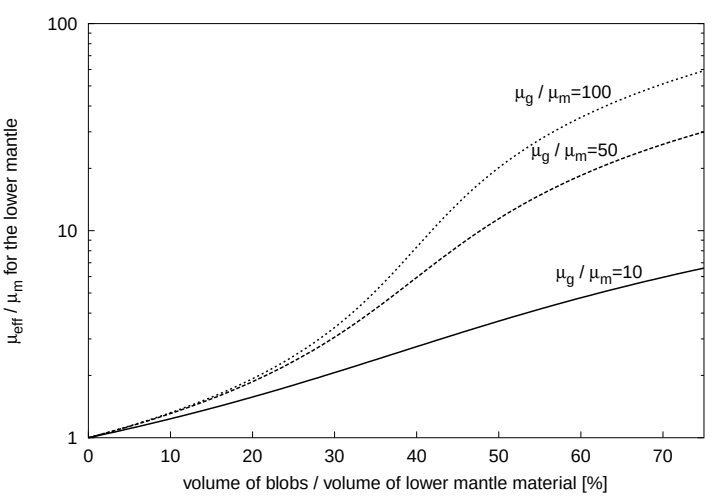


Fig. 7. Effective viscosity $\mu_{\mathrm{eff}}$ as predicted by Eq. 15 normalized by the background viscosity for different blob volume fractions $f$ and blob viscosities of $\mu_{\mathrm{b}}/\mu_{\mathrm{m}} = 10$, 50 and 100. The viscosity is assumed to be constant within the blobs for this calculation.

constraints set forth above. This volume fraction is of the order of magnitude that is needed to provide a significant reservoir of undepleted mantle material [8]. If stringent geochemical constraints confirm values on the upper end of the range, the model we propose might still work, albeit with a blob geometry that fills up the interior of the convective cells.

In the framework of our model, we can account for a maximum mantle volume fraction of 34% (65%) for case A (case B). (The correction for mass is a small one, the difference for the lower mantle being about 1.11 based on PREM.) If only blobs would produce heat at a rate $A_0$, we arrive at about $8 \times 10^{12}$ W ($15 \times 10^{12}$ W) globally. That is roughly 20% (40%) for case A (case B) of the global surface heat flux. Therefore, the heat production in the blobs alone is not sufficient to account for the global budget but secular cooling and other heat sources such as the core or the surrounding depleted mantle have to be invoked. Independent of all arguments about the Earth's heat budget we can simply state that about one (two) thirds of the mantle-based heat production could be located in the blobs for case A (B).

At this stage uncertainties in the assumptions of the geochemical models and heat budget estimates do not allow any definitive conclusions to be drawn about the blob size and the validity of our model. The lower mantle blobs could account for substantial fractions although smaller blobs (case A) seem more likely to work thermally. The order of magnitude estimation we present above leads us to conjecture that the proposed high-viscosity, slightly higher density blobs of lateral dimensions around 1200 km are possibly stable and could remain unmixed over geologically long times. We note that we have made simplifying, but necessary assumptions to arrive at analytical estimates of the physical processes. Only numerical calculations taking all the important effects (energy equation, momentum equation, deforming blobs, temperature-dependent viscosity, viscous heating, time-dependence) into account can ultimately test the feasibility of our model for the mantle.

### 3.2. Origin of high-viscosity blobs

We have shown that the model view of mantle convection with highly viscous blobs might be able to reconcile the different views of geophysics and geochemistry. One important question that remains is the origin of the blobs. They must have formed early in Earth's history in order to contain material of primitive origin. One possible rheological explanation is based on evidence that the lower mantle consists of a mixture of (Mg, Fe)$SiO_3$ perovskite (pv) and (Mg, Fe)O magnesiowüstite (mw). The melting temperatures of the two components are significantly different [35]. Since this can be interpreted as an equivalent difference in the activation energy [36], a higher ab origine fraction of perovskite within the blobs could account for higher viscosity at lower mantle depths. The intrinsic density would be increased as well (cf. Appendix A). Thus, a change in the fractions of pv and mw would also satisfy our constraint on neutral buoyancy.

It should be noted that there is nothing in the chemistry of OIBs that suggests a difference in major element chemistry relative to the depleted MORB mantle. Therefore our speculation of a pv-based mechanism for raising the viscosity does not follow directly from surface observables. However, it may take relatively small proportions of the primitive or enriched material to skew the trace element and isotopic ratios in the manner observed for OIBs. This brings us to another criticism of this model: if the blob material has such a high viscosity, how do we observe it at all? Davies' original argument involved blobs which were melted more easily due to their primitive composition and high volatile content. As discussed by Manga, however, these same features would lead to the blobs' destruction. We argue instead that the heterogeneous isotopic and trace element content of the OIBs is due to the passive entrainment of the blobs by hot upwellings. The inclusion of the primitive/enriched component in the OIBs is a function not of the blobs' physical properties but rather their geometric position in the path of the plume.

### 3.3. Observational constraints

The blobs we envision should be detectable by seismological studies such as mantle tomography [37,38] and statistical interpretations of travel-time residuals [39] or heterogeneities as shown in tomography and geodynamical models [12]. Since we are

considering blobs with an internal temperature that is higher than the ambient mantle, wave speeds can be expected to be reduced. However, as blobs are characterized by different composition and higher density as well, we expect that there is a trade-off between these two effects. There is general agreement that the effect of temperature at constant pressure is more pronounced on S-waves than on P-waves, probably by a factor of ~2 [26,40,41]. Compositional variations, on the other hand, are expected to be more pronounced in P- than in S-waves [38], one reason being the proposed difference in extrinsic and intrinsic derivatives of shear and bulk modulus [40]. The task of putting quantitative bounds on the relative partial temperature and composition derivatives of P- and S-waves $(\partial \ln v_{\mathrm{P,S}}/\partial T)|_x$ and $(\partial \ln v_{\mathrm{P,S}}/\partial x)|_T$ is complicated by many factors. The uncertainty in or lack of mineral physics data, disagreement and non-uniqueness of inversions of the average chemical composition (Si- and Fe-content) of the mantle, the estimation of effective moduli of composites and other factors together mount to large uncertainties. Having said that, we estimate reasonable numbers for the trade-off between temperature and composition. The procedure is described in the Appendix A. For the relative changes in wave speeds due to a maximum temperature increase of $\Delta T_{\max} = 300$ K at the center of the blobs we obtain:

$$\partial \ln v_{\mathrm{P}}|_x = -0.75\% \text{ and } \partial \ln v_{\mathrm{S}}|_x = -1.5\% \qquad (16)$$

(These values are reduced by a factor of about $2/3$ if the seismic rays average over the temperature distribution within the blobs, Eq. 7.) For the compositional changes caused by a higher perovskite content corresponding to an intrinsic density increase of 0.25% (counterbalancing thermal buoyancy corresponding to $\Delta T_{\max}$) we get:

$$\partial \ln v_{\mathrm{P}}|_T = 0.86\% \text{ and } \partial \ln v_{\mathrm{S}}|_T = 0.74\% \qquad (17)$$

throughout the blobs. Eqs. 16 and 17 show that the thermal and the chemical contributions to the $\mathrm{d}v_{\mathrm{P}}$ travel-time anomaly might roughly cancel out each other in the blob center while blobs might be faster than the residual mantle on average. The S-waves, on the other hand, should be slower, probably by about 0.3%. While the blobs thus tend to hide from tomography where the rays average over large volumes, blobs should be more easily detected by seismic scattering studies since the compositional contrast we propose is less offset by temperature at the blob surface.

More important than the absolute numbers for travel-time anomalies quoted above is the result that we predict an anticorrelation between P- and S-wave residuals for the lower mantle primitive blobs. Recently, tomographic studies [37,38] have moved beyond a constant scaling between P- and S-wave residuals so that travel-time residuals can be individually interpreted and the question of thermal and/or compositional anomalies readdressed. Both tomographic studies [37,38] find increasing heterogeneity and anticorrelation between shear and bulk modulus variations in the lower mantle. In addition, the spatial scales of heterogeneity have independently been determined to be on the order of 1000 km [39]. We conjecture that heterogeneities of the type we have discussed above might be at least in part responsible for the complexity seen by recent studies while the trade-off between temperature and composition might make it difficult to actually detect the existence of blobs.

## 4. Conclusion

We have shown that the proposed blob model might explain the geochemical constraints on the Earth without invoking a layered convection mode, which seems to be contradicted by geophysical evidence. Tempting as this view appears to us, the possible origin and mineralogy of the blobs and the dynamical self-consistency of the model have to be elaborated on or demonstrated. If full calculations show that the proposed model works, it would be a significant contribution to our view of mantle convection in general.

## Acknowledgements

We greatly benefited from discussions with the participants of the 1998 Harvard/MIT 'Mantle Convection' seminar. The comments of our reviewers Geoffrey F. Davies and Michael C. Gurnis as well as Michael Manga helped to improve the typescript. Th. W. B. thanks Simone Bethge for support and was

partly funded by a 'DAAD Doktorandenstipendium HSP-III'. ***[CL]***

## Appendix A. Estimation of partial temperature and composition derivatives

We estimate the relative variations in P- and S-wave speeds for changes in temperature at constant composition and vice-versa. (As usual, the logarithmic differential, e.g. $\mathrm{d}\ln v_\mathrm{P}$, is written as shorthand for relative changes in a parameter, e.g. $\mathrm{d}v_\mathrm{P}/v_\mathrm{P}$). The temperature derivatives we use are those from Stacey [26].

$$\left.\frac{\partial \ln v_\mathrm{P}}{\partial T}\right|_x = -2.5\times 10^{-5}\,\mathrm{K}^{-1} \tag{18}$$

and

$$\left.\frac{\partial \ln v_\mathrm{S}}{\partial T}\right|_x = -5.0\times 10^{-5}\,\mathrm{K}^{-1} \tag{19}$$

with a ratio of

$$\left.\frac{\partial \ln v_p}{\partial \ln v_s}\right|_x = 0.5 \tag{20}$$

They agree within the uncertainties of more recent estimates [41]. The notation $|_x$ indicates the variable that is held fixed, in this case the composition $x$. It is assumed that the temperature derivatives are appropriate for both blobs and residual mantle albeit they have different composition. Inserting the characteristic $\mathrm{d}T = \Delta T_\mathrm{max} = 300$ K from above we find that the maximal thermal changes in wave speeds in the center of the blobs amount to:

$$\mathrm{d}\ln v_\mathrm{P}|_x = -0.75\% \text{ and } \mathrm{d}\ln v_\mathrm{S}|_x = -1.5\% \tag{21}$$

In our model, the Earth's lower mantle is made of only $(\mathrm{Mg}_{1-y_\mathrm{pv}},\mathrm{Fe}_{y_\mathrm{pv}})\mathrm{SiO}_3$ perovskite and $(\mathrm{Mg}_{1-y_\mathrm{mw}},\mathrm{Fe}_{y_\mathrm{mw}})\mathrm{O}$ magnesiowüstite. By using Stacey's [42] preferred values of $y_\mathrm{pv} = 0.06$ and $y_\mathrm{mw} = 0.15$ for the Fe/(Fe + Mg) numbers of perovskite and magnesiowüstite, respectively, we reduce the compositional degrees of freedom further to the concentration of mw, denoted by $x$. The average moduli and density of a pv–mw mixture are calculated based on the preferred $x_0 = 0.28$ from [42] at zero pressure and room temperature. We assume that the logarithmic derivatives with respect to $x$ that we then derive for these conditions are roughly the same as the derivatives at higher pressure and temperatures for the lower mantle. This assumption should hold to first order since incompressibilities $K$ (and thus to first order also $\rho$) have about the same pressure derivatives for pv and mw [43]. We therefore assume that the ratios between the relevant parameters for both minerals stay roughly the same independent of the reference depth.

Wang and Weidener [41] state the densities of pv and mw as:

$$\rho_0^\mathrm{pv} = 4108 + 1070 y_\mathrm{pv}\,[\mathrm{kg/m^3}] \tag{22}$$

and

$$\rho_0^\mathrm{mw} = 3583 + 2280 y_\mathrm{mw}\,[\mathrm{kg/m^3}] \tag{23}$$

which for our composition result in

$$\rho_0^\mathrm{pv} = 4172\,\mathrm{kg/m^3} \text{ and } \rho_0^\mathrm{mw} = 3925\,\mathrm{kg/m^3} \tag{24}$$

so that

$$\rho_0 = (1-x)\rho_0^\mathrm{pv} + x\rho_0^\mathrm{mw} = 4103\,\mathrm{kg/m^3} \tag{25}$$

Differentiating Eq. 25 gives:

$$\left.\frac{\partial \ln \rho}{\partial x}\right|_T = \frac{\rho_\mathrm{mw}-\rho_\mathrm{pv}}{\rho_\mathrm{pv}+x(\rho_\mathrm{mw}-\rho_\mathrm{pv})} = -0.06 \tag{26}$$

for the relative changes in average density at constant $T$. One can compare this value with $(\partial \ln\rho/\partial T)|_x$ which is simply the thermal expansion coefficient $\alpha$.

Turning to the bulk modulus, we use the adiabatic values for the mineral components from [41] and [43]

$$K_\mathrm{pv}^\mathrm{S} = 264\,\mathrm{GPa} \text{ and } K_\mathrm{mv}^\mathrm{S} = 163\,\mathrm{GPa} \tag{27}$$

as a start. Various methods of estimating the bulk modulus of the assemblage have been proposed while the final answers for $K_0$ differ only slightly [43]. We follow the self-consistent approach which was already used for the effective viscosity of the blob-filled mantle. The counterpart of Eq. 15 for $K_0$ — written with mw as a component with volume fraction $x$ in the pv matrix — is [34]:

$$\frac{x}{1-\gamma(K_\mathrm{mv}/K_0-1)} + \frac{1-x}{1+\gamma(K_\mathrm{pv}/K_0-1)} = 1 \tag{28}$$

A factor $\gamma$ entered the equation that depends on the composite's Poisson ratio $\nu^*$:

$$\gamma = \frac{1+\nu^*}{3(1-\nu^*)} \tag{29}$$

The corresponding equation for the composite shear modulus $G_0$ is:

$$\frac{x}{1+\beta(G_\mathrm{mv}/G_0-1)} + \frac{1-x}{1+\beta(G_\mathrm{pv}/G_0-1)} = 1 \tag{30}$$

with

$$\beta = \frac{2(4-\nu^*)}{15(1-\nu^*)} \tag{31}$$

$\nu^*$ couples Eqs. 28 and 30, and it is readily seen that the formula for the effective viscosity, Eq. 15, follows from Eq. 30 with $\nu^* \to 1/2$. We can solve the system for $K_0$ as a function of $G_\mathrm{mv}$, $G_\mathrm{pv}$, $K_\mathrm{mv}$, $K_\mathrm{pv}$ and $x$. It turns out that the exact solution is rather cumbersome and we will not give it here. We will, however, give the formula that results when we set $\nu^* = 1/3$ as a reasonable number for the composite material:

$$K_0 \approx \tfrac{1}{2}\left\{(3x-2)K_\mathrm{mv} + (1-3x)K_\mathrm{pv} + \left[8K_\mathrm{mv}K_\mathrm{pv} + \left((2-3x)K_\mathrm{mw} + (3x-1)K_\mathrm{pv}\right)^2\right]^{1/2}\right\} \tag{32}$$

The logarithmic derivative of Eq. 32 is:

$$\left.\frac{\partial \ln K}{\partial x}\right|_T \approx 3(K_\mathrm{mv}-K_\mathrm{pv}) \times \left\{8K_\mathrm{mv}K_\mathrm{pv} + ((3x-2)K_\mathrm{mv} + (1-3x)K_\mathrm{pv})^2\right\}^{1/2} \tag{33}$$

Uncertainties about the shear modulus $G$ are far greater than for $K$. From Wang and Weidener [41] we get the estimates:

$$G_{\rm pv} = 177\,{\rm GPa} \;\text{ and }\; G_{\rm mw} = 120\,{\rm GPa} \tag{34}$$

As in the case for $K$, we can simplify the solution of Eqs. 28 and 30 with $\nu^* = 1/3$. Then,

$$G_0 \approx \tfrac{1}{16}\Big\{(15x-7)G_{\rm mv} + (8-15x)G_{\rm pv} + \big[224G_{\rm mv}G_{\rm pv} + ((7-15x)G_{\rm mw} + (15x-8)G_{\rm pv})^2\big]^{1/2}\Big\} \tag{35}$$

and

$$\left.\frac{\partial \ln G}{\partial x}\right|_T \approx 15(G_{\rm mv} - G_{\rm pv}) \times \left\{224G_{\rm mv}G_{\rm pv} + ((15x-7)K_{\rm mv} + (8-15x)G_{\rm pv})^2\right\}^{1/2} \tag{36}$$

follows. Eqs. 32 and 35 can be compared with the effective viscosity, Eq. 15.

The exact solution of Eqs. 28 and 30 for the numbers given in Eqs. 27 and 34 is:

$$K_0 = 225\,{\rm GPa} \;\text{ and }\; G_0 = 160\,{\rm GPa} \tag{37}$$

for the moduli and

$$\left.\frac{\partial \ln K}{\partial x}\right|_T = -0.53 \;\text{ and }\; \left.\frac{\partial \ln G}{\partial x}\right|_T = -0.41 \tag{38}$$

for the relative derivatives of the moduli with respect to changing composition at constant temperature. These numbers are within a few percent of our simplified formulas of symmetric form Eqs. 32, 33, 35 and 36 which gives them a posteriori justification. One has to bear in mind that the uncertainties about the input data are probably much larger than those of the approximations made here. However, Eq. 38 indicates that our assessment indicates a stronger (factor 1.3) $x$-dependence of $K$ than of $G$ as was expected.

For isotropic media:

$$\mathrm{d}\ln v_{\rm P} = \frac{1}{2}\left\{\frac{K}{K+\frac{4}{3}G}\mathrm{d}\ln K + \frac{G}{G+\frac{3}{4}K}\mathrm{d}\ln G - \mathrm{d}\ln\rho\right\} \tag{39}$$

and

$$\mathrm{d}\ln v_{\rm S} = \tfrac{1}{2}(\mathrm{d}\ln G - \mathrm{d}\ln\rho) \tag{40}$$

holds. We now consider only compositional variations so that e.g. $\mathrm{d}\ln K = (\partial \ln K/\partial x)|_T \mathrm{d}x$. If we then substitute the zero pressure values of $K$ and $G$ into Eqs. 39 and 40,: we arrive at

$$\left.\frac{\partial \ln v_{\rm P}}{\partial x}\right|_T = -0.21 \tag{41}$$

and

$$\left.\frac{\partial \ln v_{\rm S}}{\partial x}\right|_T = -0.18 \tag{42}$$

with a ratio of

$$\left.\frac{\partial \ln v_{\rm P}}{\partial \ln v_{\rm S}}\right|_T = 1.2 \tag{43}$$

for the dependence of the seismic wave speeds on composition variations $\mathrm{d}x$. Since $v_{\rm P}$ is a function of $G$ and $K$, Eq. 43 is a slightly weaker indicator for compositional heterogeneity than the ratio of the moduli derivatives, Eq. 38.

We continue with our estimate from above that excess thermal buoyancy due to $\Delta T_{\rm max} \approx 300$ K can be counterbalanced by a compositional density contrast of $\mathrm{d}\ln\rho \approx 0.25\%$ (cf. Eq. 10). By Eq. 26 we can account for an increase of that order when the composition is shifted towards a higher perovskite content by about $\mathrm{d}x = -0.041$. Then, from Eq. 38, $\mathrm{d}\ln K = 2.2\%$ and $\mathrm{d}\ln G = 1.7\%$ and finally with Eq. 42:

$$\mathrm{d}\ln v_{\rm P}|_T = 0.86\% \;\text{ and }\; \mathrm{d}\ln v_{\rm S}|_T = 0.74\% \tag{44}$$

follows for the change in wave speeds within blobs whose mv content is decreased from $x = 28\%$ to $x = 23.9\%$. As stated above, we proceed under the assumption that at least the order of magnitude and the ratio $(\partial \ln v_{\rm P}/\partial \ln v_{\rm S})|_T$ given by Eq. 43 is meaningful for lower mantle conditions. We thus have demonstrated that changes in temperature will effect $v_{\rm S}$ more than $v_{\rm P}$ while the opposite is true for compositional changes.

## References


[1] B. Dupre, C.J. Allègre, Pb–Sr isotope variation in Indian Ocean basalts and mixing phenomena, Nature 303 (1983) 142–146.

[2] M. Gurnis, Quantitative bounds on the size spectrum of isotopic heterogeneity within the mantle, Nature 323 (1986) 317–320.

[3] C.J. Allègre, D.L. Turcotte, Implications of a two-component marble-cake mantle, Nature 323 (1986) 123–127.

[4] A. Zindler, S.R. Hart, Chemical geodynamics , Annu. Rev. Earth Planet. Sci. 14 (1986) 493–571.

[5] M.D. Kurz, W.J. Jenkins, S.R. Hart, D. Clague, Helium isotopic variations in volcanic rocks from Loihi Seamount and the Island of Hawaii, Earth Planet. Sci. Lett. 66 (1983) 388–406.

[6] K.A. Farley, J.H. Natland, H. Craig, Binary mixing of enriched and undegassed (primitive-questionable) mantle components (He, Sr, Nd, Pb) in Samoan lavas, Earth Planet. Sci. Lett. 111 (1992) 183–199.

[7] S.R. Hart, A. Zindler, Constraints on the nature and development of chemical heterogeneities in the mantle, in: W.R. Peltier (Ed.), Mantle Convection: Plate Tectonics and Global Dynamics, Gordon and Breach, New York, 1989, pp. 261–387.

[8] S. Jacobsen, G. Wasserburg, The mean age of mantle and crustal reservoirs, J. Geophys. Res. 84 (1979) 7411–7427.

[9] C.J. Allègre, A. Hofmann, K. O'Nions, The Argon constraints on mantle structure, Geophys. Res. Lett. 23 (1996) 3555–3557.

[10] G.F. Davies, Geophysically constrained mantle mass flows and the $^{40}$Ar budget: a degassed lower mantle?, Earth Planet. Sci. Lett. 166 (1999) 149–162.

[11] H.-P. Bunge, M.A. Richards, J.R. Baumgardner, Effect of depth-dependent viscosity on the planform of mantle convection, Nature 379 (1996) 436–438.
[12] P. Puster, T.H. Jordan, How stratified is mantle convection?, J. Geophys. Res. 102 (1997) 7625–7646.
[13] R.D. van der Hilst, S. Widiyantoro, E.R. Engdahl, Evidence of deep mantle circulation from global tomography, Nature 386 (1997) 578–584.
[14] S.P. Grand, R.D. van der Hilst, S. Widiyantoro, Global seismic tomography; a snapshot of convection in the Earth, GSA Today 7 (1997) 1–7.
[15] F. Albarède, Time-dependent models of the U–Th–He and K–Ar evolution and the layering of mantle convection, Chem. Geol. 145 (1998) 413–429.
[16] P.G. Silver, R.W. Carlson, P. Olson, Deep slabs, geochemical heterogeneity, an the large-scale structure of mantle convection: investigation of an enduring paradox, Annu. Rev. Earth Planet. Sci. 16 (1988) 477–541.
[17] G.F. Davies, M.A. Richards, Mantle convection, J. Geol. 100 (1992) 151–206.
[18] G.F. Davies, Geophysical and isotopic constraints on mantle convection: an interim synthesis, J. Geophys. Res. 89 (1984) 6017–6040.
[19] B.H. Hager, Subducted slabs and the geoid: constraints on mantle rheology and flow, J. Geophys. Res. 89 (1984) 6003–6015.
[20] M. Gurnis, G.F. Davies, The effect of depth-dependent viscosity on convective mixing in the mantle and the possible survival of primitive mantle, Geophys. Res. Lett. 13 (1986) 541–544.
[21] P. van Keken, C.J. Ballentine, Whole-mantle versus layered mantle convection and the role of a high-viscosity lower mantle in terrestrial volatile evolution, Earth Planet. Sci. Lett. 156 (1998) 19–32.
[22] S. Ferrachat, Y. Ricard, Regular vs. chaotic mantle mixing, Earth Planet. Sci. Lett. 155 (1998) 75–86.
[23] J.B. Kellogg, R.J. O'Connell, Toroidal motion and mixing in three dimensions, EOS 79 (1998) S334.
[24] M. Manga, Mixing of heterogeneities in the mantle: effect of viscosity differences, Geophys. Res. Lett. 23 (1996) 403–406.
[25] M. Manga, Interactions between mantle diapirs, Geophys. Res. Lett. 24 (1997) 1871–1874.
[26] F.D. Stacey, Physics of the Earth (3rd ed.), Brookfield Press, Kenmore, Australia, 1992.
[27] A.M. Dziewonski, D.L. Anderson, Preliminary reference Earth model, Phys. Earth Planet. Inter. 25 (1981) 297–356.
[28] G. Ranalli, Rheology of the Earth (2nd ed.), Chapman and Hall, London, 1995.
[29] W.F. McDonough, S.-s. Sun, The composition of the earth, Chem. Geol. 120 (1995) 223–253.
[30] H.S. Carslaw, J.C. Jaeger, Conduction of Heat in Solids (2nd ed.), Oxford University Press, London, 1959, p. 243.
[31] S.E. Kesson, J.D. Fitz Gerald, J.M. Shelley, Mineralogy and dynamics of a pyrolite lower mantle, Nature 393 (1998) 252–254.
[32] S.-i. Karato, Rheology of the lower mantle, Phys. Earth Planet. Inter. 24 (1981) 1–14.
[33] A.P. van den Berg, D.A. Yuen, The role of shear heating in lubricating mantle flow, Earth Planet. Sci. Lett. 151 (1997) 33–42.
[34] N. Laws, R. McLaughlin, Self-consistent estimates for the viscoelastic creep compliances of composite materials, Proc. R. Soc. London A 359 (1978) 251–273.
[35] A. Zerr, R. Boehler, Constraints on the melting temperature of the lower mantle from high-pressure experiments on MgO and magnesiowustite, Nature 371 (1994) 506–508.
[36] J. Weertman, The creep strength of the Earth's mantle, Rev. Geophys. Space Phys. 8 (1970) 145–168.
[37] W.-j. Su, A.M. Dziewonski, Simultaneous inversion for 3-D variations in shear and bulk velocity in the mantle, Phys. Earth Planet. Inter. 100 (1997) 135–156.
[38] B.L.N. Kennett, S. Widiyantoro, R.D. van der Hilst, Joint seismic tomography for bulk sound and shear wave speed in the Earth's mantle, J. Geophys. Res. 103 (1998) 12469–12493.
[39] J.H. Davies, O. Gudmundsson, R.W. Clayton, Spectra of mantle shear wave velocity structure, Geophys. J. Int. 108 (1992) 565–582.
[40] D.L. Anderson, A seismic equation of state, II, Shear properties and thermodynamics of the lower mantle, Earth Planet. Sci. Lett. 45 (1987) 307–323.
[41] Y. Wang, D.J. Weidner, $(\partial\mu/\partial t)_p$ of the lower mantle, Pure Appl. Geophys. 146 (1996) 533–549.
[42] F.D. Stacey, Thermoelasticity of (Mg, Fe)$SiO_3$ perovskite and a comparison with the lower mantle, Phys. Earth Planet. Inter. 98 (1996) 65–77.
[43] F.D. Stacey, Thermoelasticity of a mineral composite and a reconsideration of lower mantle properties, Phys. Earth Planet. Inter. 106 (1998) 219–236.